Science Bulletin 65 (2020) 1643–1649

Contents lists available at ScienceDirect

Science Bulletin

journal homepage: www.elsevier.com/locate/scib

Science Bulletin
www.scibull.com

Article

Transmission electron microscopy of organic-inorganic hybrid perovskites: myths and truths

Shulin Chen [a,b], Ying Zhang [c], Jinjin Zhao [c,*], Zhou Mi [c], Jingmin Zhang [a], Jian Cao [b], Jicai Feng [b], Guanglei Zhang [c], Junlei Qi [b,*], Jiangyu Li [d,g,*], Peng Gao [a,e,f,*]

[a] Electron Microscopy Laboratory, School of Physics, Peking University, Beijing 100871, China
[b] State Key Laboratory of Advanced Welding and Joining, Harbin Institute of Technology, Harbin 150001, China
[c] School of Materials Science and Engineering, School of Mechanical Engineering, Shijiazhuang Tiedao University, Shijiazhuang 050043, China
[d] Shenzhen Key Laboratory of Nanobiomechanics, Shenzhen Institutes of Advanced Technology, Chinese Academy of Sciences, Shenzhen 518055, China
[e] Collaborative Innovation Center of Quantum Matter, Beijing 100871, China
[f] International Center for Quantum Materials, School of Physics, Peking University, Beijing 100871, China
[g] Department of Materials Science and Engineering, Southern University of Science and Technology, Shenzhen 518055, China

ARTICLE INFO

Article history:
Received 15 February 2020
Received in revised form 22 April 2020
Accepted 18 May 2020
Available online 23 May 2020

Keywords:
Organic-inorganic hybrid perovskites
Transmission electron microscopy
Beam damage mechanism
Atomic structure $CH_3NH_3PbI_3$
Facet dependency

ABSTRACT

Organic-inorganic hybrid perovskites (OIHPs) have attracted extensive research interest as a promising candidate for efficient and inexpensive solar cells. Transmission electron microscopy (TEM) characterizations that can benefit the fundamental understanding and the degradation mechanism are widely used for these materials. However, their sensitivity to the electron beam illumination and hence structural instabilities usually prevent us from obtaining the intrinsic information or even lead to significant artifacts. Here, we systematically investigate the structural degradation behaviors under different experimental factors to reveal the optimized conditions for TEM characterizations of OIHPs by using low-dose electron diffraction and imaging techniques. We find that a low temperature (−180 °C) does not slow down the beam damage but instead induces a rapid amorphization for OIHPs. Moreover, a less severe damage is observed at a higher accelerating voltage. The beam-sensitivity is found to be facet-dependent that a (1 0 0) exposed $CH_3NH_3PbI_3$ ($MAPbI_3$) surface is more stable than a (0 0 1) surface. With these guidance, we successfully acquire the atomic structure of pristine $MAPbI_3$ and identify the characterization window that is very narrow. These findings are helpful to guide future electron microscopy characterizations of these beam-sensitive materials, which are also useful for finding strategies to improve the stability and performance of the perovskite solar cells.

1. Introduction

Organic-inorganic hybrid perovskites (OIHPs) have achieved impressive improvements as promising photovoltaic materials, whose power conversion efficiency rapidly increases from initial 3.8% [1] to most recent 25.2% [2]. However the commercialization of the technology is still hindered by the poor long-term stability issues [3,4]. Transmission electron microscopy (TEM)-based studies benefit the fundamental understanding of their nature, functionality as well as the degradation mechanism for these fascinating materials [5,6], which makes great contribution to the development OIHPs based solar cells. OIHPs are extremely sensitive to the electron beam [7,8]. It is reported that the high energy electron beam at 300 kV has already caused damage within 100 e $Å^{-2}$ and induced the degradation from $CH_3NH_3PbI_3$ ($MAPbI_3$) to PbI_2 within 2200 e $Å^{-2}$ [7]. However, many studies ignored such electron beam sensitivity. Thus, even for basic phase identifications by relatively low dose electron diffraction (ED) technique, many researchers mistakenly identified the PbI_2 as $MAPbI_3$ [9–16]. The situation for *in situ* TEM studies on OIHPs is even worse since under common high resolution TEM (HRTEM) (dose rate: thousands of e $Å^{-2}$ s^{-1}) or high-angle annular dark field scanning TEM (STEM) (dose rate: hundreds or thousands of e $Å^{-2}$ s^{-1}) imaging modes, the total doses within several seconds are large enough to induce damage or full decomposition, likely leading to inaccurate or even incorrect conclusions (see Table S1 online for detailed discussion). For example, Segawa group [17] used *in situ* HRTEM patterns to record the microstructural changes of $MAPbI_3$ for 5 min. At such

* Corresponding authors.
E-mail addresses: jinjinzhao2012@163.com (J. Zhao), jlqi@hit.edu.cn (J. Qi), jy.li1@siat.ac.cn (J. Li), p-gao@pku.edu.cn (P. Gao).

https://doi.org/10.1016/j.scib.2020.05.020
2095-9273/

a high dose, the sample is likely PbI_2 rather than $MAPbI_3$ thus the observed structural changes are likely mainly due to the electron beam irradiation instead of temperature effect. Also, Divitini et al. [11] observed the heat-induced structural and chemical changes by *in situ* heating, however both the sample preparation by focused ion beam and STEM imaging mode can cause large damage or complete decomposition, as a result the ion migration under heating likely takes place in PbI_2 rather than $MAPbI_3$. *In situ* electrical biasing TEM experiments by Jeangros et al. [18] and Jung et al. [19] also ignored the beam sensitivity of OIHPs. Therefore, it is highly desirable to investigate and clarify the effect of the electron beam itself on the structure instability so that we can draw valid conclusions from the TEM characterizations, especially under external stimuli by *in situ* TEM.

So far, not too many literatures have been devoted to investigating the effect of the electron beam illumination on OIHPs in TEM [7,20–22]. Rothmann et al. [22] noticed the dose rate for these extremely beam-sensitive materials and acquired selected area electron diffraction (SAED) pattern from the intrinsic $MAPbI_3$ at a low dose rate 1 e $Å^{-2}$ s^{-1}. Chen et al. [7] uncovered that the structure damage has already been induced within 100 e $Å^{-2}$ s^{-1} and proposed a detailed decomposition pathway for single crystalline $MAPbI_3$. Recently, Alberti et al. [20] unveiled a Pb-clusters related degradation mechanism for polycrystalline $MAPbI_3$ films. Besides these studies based on the ED patterns, Zhang et al. [23] acquired the structure of $CH_3NH_3PbBr_3$ ($MAPbBr_3$) with extremely low doses using direct-detection electron-counting camera. These TEM studies showed that dozens of e $Å^{-2}$ doses are able to induce damage or even decomposition for OIHPs, preventing atomic-scale investigation as well as *in situ* study under external stimuli. To minimize radiation damage effect, Li et al. [8] retrieved the structure of $MAPbI_3$ by cryo-electron microscopy (cryo-EM), highlighting the importance of low temperature for beam sensitive material characterization. However, this is inconsistent with Rothmann's study that a low temperature causes a rapid amorphization [21]. Thus whether or not the low temperature is beneficial for EM characterizations of OIHPs is still unclear. Furthermore, what kind of factors influence the beam sensitivity and how to increase the total damage-free doses during characterizations have been rarely explored and thus motivate this study.

In this work, we study the effect of external factors (temperature, accelerating voltage) and internal factors (exposed facets) on the structural instabilities of OIHPs under electron beam irradiation. It is found that a low temperature (−180 °C) causes a rapaid crystal-amorphous transition within low doses (129 to 150 e $Å^{-2}$), suggesting that low temperature is not helpful in preventing the electron beam damage while a high temperature (90 °C) does not change the degradation pathway observed at room temperature (RT). The beam damage mechanism is identified to be radiolysis since a high voltage is beneficial to reduce the damage. Besides we reveal that the beam-sensitivity is facet-dependent, with a (1 0 0) exposed $MAPbI_3$ surface more stable than a (0 0 1) surface. We also acquire the atomic structure of $MAPbI_3$ at an extremely low dose. Our findings can guide future EM characterizations of these beam-sensitive materials and also lay a foundation for the in-depth decomposition study under various stimuli by EM.

2. Experimental

2.1. $CH_3NH_3PbI_3$ single crystalline film fabrication

PbI_2 and CH_3NH_3I (molar ratio 1:1) were dissolved in γ-butyrolactone (GBL) with the concentration of 1.3 mol L^{-1}, prior to stirring in 12 h at the 70 °C. The $MAPbI_3$ precursor solution was obtained and filtered using polytetrafluoroethylene (PTFE) filter with 0.22 μm pore size. The fluorine-doped tin oxide (FTO)/TiO_2 substrates [24] were face-to-face clamped together at fixed distance of 50–200 μm. The fixed FTO/TiO_2 substrates were vertically and partially soaked in a 10 mL $MAPbI_3$ precursor solution at 120 °C, and then the feeding $MAPbI_3$ precursor solution was added twice a day in the nitrogen glove box. The perovskite solution climbed along the pores of the mesoporous TiO_2 substrate from bottom to top and covered the entire substrate, and then crystallized into a film due to the temperature difference, forming the single crystal film [7,24]. After some days, the substrates with $MAPbI_3$ single crystal film were taken out, and then dried at 120 °C for 10 min in nitrogen.

2.2. $CH_3NH_3PbBr_3$ single crystal preparation

$PbBr_2$ and CH_3NH_3Br were dissolved in *N*,*N*-dimethylformamide (DMF) and stirred at 30 °C for 12 h to obtain 1 mol L^{-1} $MAPbBr_3$ precursor solution. The $MAPbBr_3$ precursor solution was purified by PTFE filter with 0.22 μm pore size, and then heated to 95 °C in a 10 mL container in dark environment. The container can be taken out by daylight at 30%–50% humidity until the $MAPbBr_3$ single crystals were grown after one night [25].

2.3. TEM samples preparation

To avoid side reactions, all TEM samples were prepared in an argon-filled glovebox. We firstly scratched samples from substrate and dispersed them into anhydrous ether. Then, the clear suspensions were deposited on holey carbon copper girds. We sealed the carbon copper girds with a plastic bag full of argon before transformed into the TEM column. The water concentration inside the plastic bag is below 0.1 ppm. The perovskite powders were exposed inside the plastic bag for about 5 min during the transport of perovskite sample.

2.4. Characterization

Powder X-ray diffraction (XRD) patterns were obtained on D8 Advance diffractometer using Cu Kα radiation (40 kV and 40 mA) with a scanning rate of 4° min^{-1} for wide-angle test increment. The HRTEM and the SAED patterns were conducted at an aberration corrected FEI (Titan Cubed Themis G2) operated at 80 and 300 kV. The energy dispersive X-ray spectroscopy (EDS) was carried out at 300 kV, 10–20 pA, (0.5–1) × 10^3 counts per second for 120 s. The cooling and heating experiments were performed at FEI Tecnai F20 at 200 kV by a liquid nitrogen side-entry specimen holder (Gatan 636). The temperature is stable at the expected value for 1 h before turning on the illumination to record data. As for all SAED images, it takes about 30 s to get the first SAED patterns since the sample comes into sight. The HRTEM images of the $MAPbI_3$ were acquired at a magnification of 71,000 by Gatan K2 direct-detection camera in the electron-counting mode with the dose fractionation function. The simulated ED patterns were obtained by the Single Crystalmaker software.

3. Results and discussion

To study the effect of temperature on the beam sensitivity, we first examine the phase of $MAPbI_3$ at different temperature, which is reported to be orthorhombic phase below −(111 ± 2) °C, tetragonal phase between −(111 ± 2) and (58 ± 5) °C and cubic phase over (58 ± 5) °C [26,27], as shown in Fig. 1a–c. The $MAPbI_3$ is grown to be a tetragonal phase (Fig. S1 online) [24], whose SAED pattern (Fig. 1e) matches with the simulated one (Fig. 1h). At −180 °C, the acquired SAED pattern (Fig. 1d) shows no superstucture diffraction

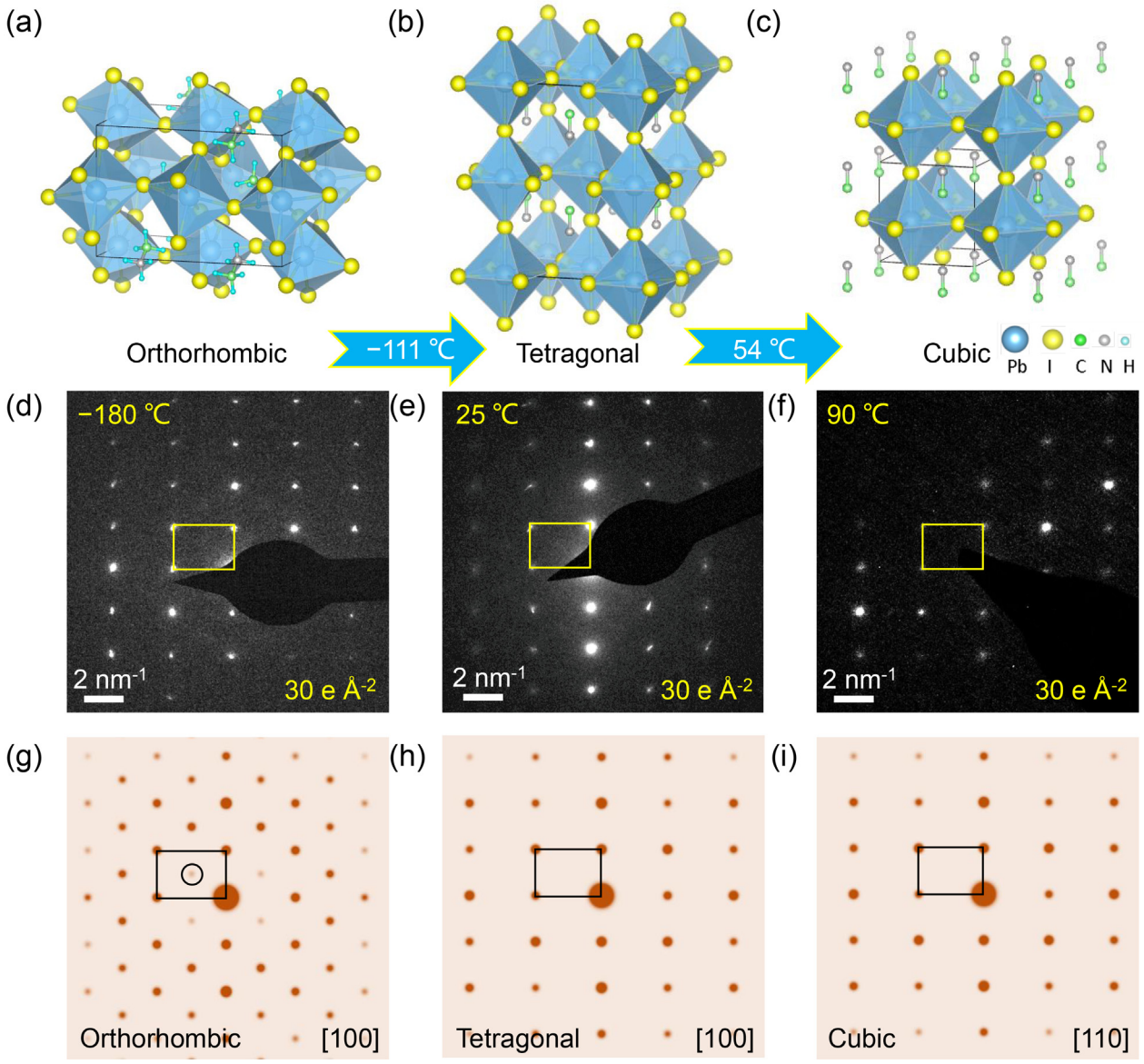

Fig. 1. (Color online) Phases characterization of $MAPbI_3$ under different temperature. Atomistic structures of (a) orthorhombic (below −111 °C), (b) tetragonal (−111 to 54 °C) and (c) cubic (over 54°C) $MAPbI_3$. (d–f) SAED patterns of $MAPbI_3$ at −180, 25, 90 °C. (g–i) The corresponding simulated SAED patterns along the [1 0 0] direction of orthorhombic and tetragonal $MAPbI_3$ and [1 1 0] direction of cubic $MAPbI_3$.

spots of the orthorhombic phase, highlighted by the circle on the simulated ED pattern (Fig. 1g), suggesting that a low temperature in vacuum will not cause the transition from tetragonl to orthorhombic phase for the single crystal $MAPbI_3$, which has also been observed in Diroll's study [28]. We also examine the phase at a high temperature and find the SAED pattern at 90 °C (Fig. 1f) indicates either a [1 1 0] direction of cubic phase (Fig. 1i) or a [1 0 0] direction of the tetragonal phase (Fig. 1h), thus making us unable to indentify the specific phase. Since the obtained SAED patterns can match with the pristine $MAPbI_3$, it is concluded the structure of $MAPbI_3$ is not damaged under low and high temperature in vacuum.

Then we further investigate the degradation pathway at −180, 25 and 90 °C to reveal the effect of temperature on the beam sensitivity as shown in Fig. 2. At −180 °C, the SAED pattern (Fig. 2a) is identified to be a [0 0 1] zone axis of tegragonal $MAPbI_3$ with additional superstucture diffraction spots marked by the circles, which are possibly caused by the ordered iodine vacancies [7]. With increased doses, the sharp diffraction reflections continuously disappear and finally change into an amorphous ring within 150 e $Å^{-2}$ (Fig. 2b–d), indicating a crystal-amorphous transition. The HRTEM image of the amorphous phase is shown in Fig. S2 (online). Compariably, a crystal-crystal transition from $MAPbI_3$ to PbI_2 is observed at 25 °C (Fig. 2e–h), whose degradation pathway starts with the loss of ordered halogen ions, followed by the loss of remaining halogen and methylamine ions, leading to final decomposition into PbI_2, as we reported before [7]. From [1 0 0] direction of tetragonal $MAPbI_3$, we again observe such crystal-amorphous transition at −180 °C within 129 e $Å^{-2}$ and a crystal-crystal transition at 25 °C (Fig. S3 online). When temperature increases to 90 °C, $MAPbI_3$ can maintain its stucture within 38 e $Å^{-2}$ (Fig. S4 online), and the observed degradation pathway (Fig. 2i–l) is consistent with that at 25 °C, which is through an intermidate phase to the final PbI_2. Fig. 2m presents the total doses to observe the appearance of superstructure, transformation into amorpous phase and PbI_2 at different tempearture. At −180 °C, the doses for generating superstructure (below 30 e $Å^{-2}$) and crystal-amorphous transition (150 e $Å^{-2}$) are smaller than 35 and 475 e $Å^{-2}$

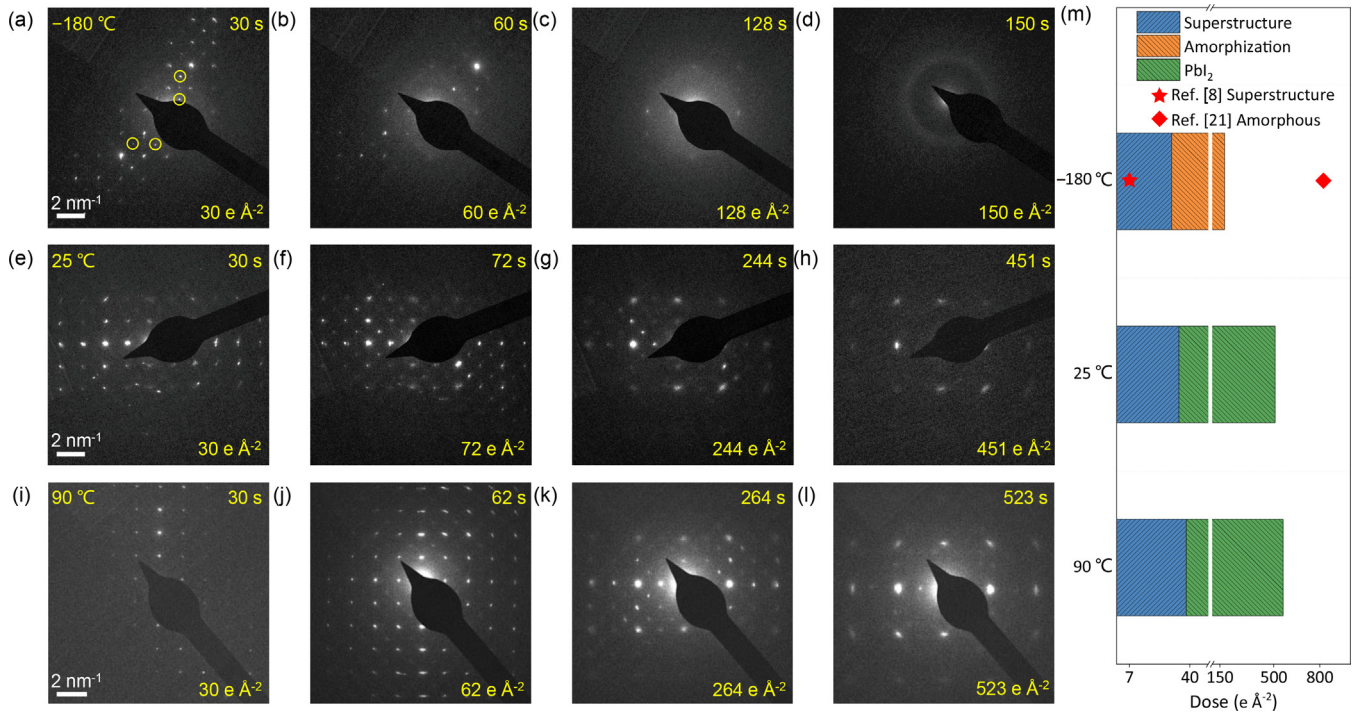

Fig. 2. (Color online) The effect of temperature on the beam sensitivity of $MAPbI_3$. Time-series SAED patterns along the [0 0 1] direction showing the degradation pathway at (a–d) −180 °C, (e–h) 25 °C, (i–l) 90 °C. The dose rate is 1 e $Å^{-2}$ s^{-1} at 200 kV. (m) The critical doses to observe the appearance of superstructure phase, transformation into amorphous phase and PbI_2. The doses marked by pentagram and rhombus are 7.6 and 820 e $Å^{-2}$.

(transformation into PbI_2) at 25 °C and 38 and 523 e $Å^{-2}$ (transformation into PbI_2) at 90 °C, suggesting $MAPbI_3$ is less stable at low temperature under electron beam irradiation. In fact, the data from earlier cryo-EM study also showed the formation of superstructure at 7.6 e $Å^{-2}$ [8], although it was not discussed, and their dose is too low to observe amorphous transition. Rothmann et al. [21], on the other hand, observed crystal-amorphous transition in polycrystalline $MAPbI_3$ film, while no superstructure has been observed. The total dose for becoming amorphous (~820 e $Å^{-2}$) in their study is larger than that in our case (150 e $Å^{-2}$), likely due to the enhanced stability with the appearance of orthorhombic phase in tetragonal phase [29]. Such amorphization transition only occurs at low temperature. It should also be noted that although the dose for transforming into PbI_2 at 90 °C (523 e $Å^{-2}$) is slightly larger than that at 25 °C (451 e $Å^{-2}$), cosidering the possible variations of sample conditions such as different thickness [10] and crystalline quality from one specimen to another, it does not necessarily suggest a higher stability for $MAPbI_3$ at 90 °C.

To comfirm the generalizaiton of such crystal-amorphous transition at −180 °C, we also investigate the structure evolution of cubic $MAPbBr_3$ (Fig. S5 online) at different temperature as shown in Fig. S6 (online). With increased dose, $MAPbBr_3$ gradually decomposes to form intermediate phase with superstructure reflections similar to $MAPbI_3$, and eventually decomposes into final $PbBr_2$ (Fig. S6e–h online). Compariably, at −180 °C, the sharp diffraction spots disappear quickly during the contious electron beam irradiation and finaly become diffused diffraction ring within 81 e $Å^{-2}$ (Fig. S6a–d online), again indicating a crystal-amorphous transition, which has also been observed in pure inorganic halide perovskite $CsPbBr_3$ [30]. We have carried out the EDS experiment to determine the composition of such amorphous phase at −180 °C as shown in Fig. S7 (online), which suggests the formation of Pb and $PbBr_2$ with negligible signal of N and C. However, the composition may be different from initial amorphous material due to the large electron dose illumination during the EDS measurement. Therefore, for both tetragonal $MAPbI_3$ and cubic $MAPbBr_3$, low temperature can not suppress the beam damage but cause a rapid crystal-amorphous transition. This is because under the electron beam irradiation, many defects (interstitials and vacancies) can be generated, which are mobile or form other quasi-stable configurations, causing new kinds of order at RT [31]. However the atomic defects are frozen and much less mobile [32,33] at low temperature, thus they are prone to be accumulated as clusters, further becoming amorphous [21].

Besides temperature, accelerating voltage is another important factor concerning about beam sensitivity during TEM characterization. The total doses (D_t) before the superstructure spots appear is used as a reference to determine the beam sensitivity. We acquire the D_t at 80 and 300 kV from samples on the same TEM grid. As shown in Fig. 3, the D_t at 300 kV (38–39 e $Å^{-2}$) is about 2–3 times larger than that at 80 kV (13–16 e $Å^{-2}$) and the raw data is shown

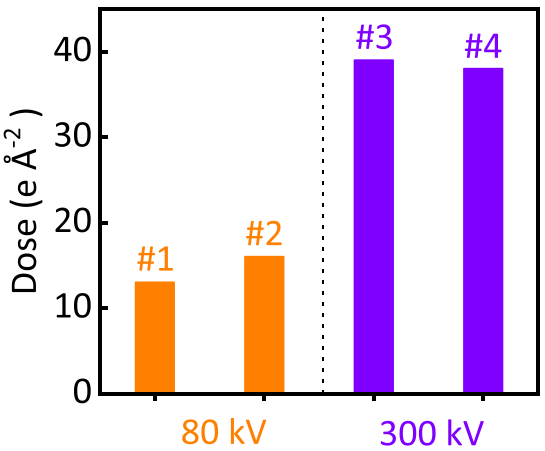

Fig. 3. (Color online) The effect of voltage and electron beam damage mechanism. The measured D_t values at 80 and 300 kV of $MAPbI_3$, indicating a radiolysis mechanism that a high voltage can decrease the damage. The dose rate is 0.2 e $Å^{-2}$ s^{-1} for #1–3 and 0.4 e $Å^{-2}$ s^{-1} for #4.

in Fig. S8 (online), which suggests EM characterizations of OIHPs at a high voltage is helpful to reduce the damage. The smaller damage at a higher voltage also indicates knock-on damage is not the main damage mechanism since a higher energy incident electron is expected to cause a severer knock-on damage [34,35]. The data recorded at 200 kV (Fig. S9 online) presents consistent conclusion that higher voltage brings in smaller damage. Moreover, lowering temperature should help reduce the damage for heating damage mechanism but instead it is observed a rapid crystal-amorphous transition. Thus the damage mechanism for $MAPbI_3$ is identified to be radiolysis, which is consistent with its semi-conduct nature [36].

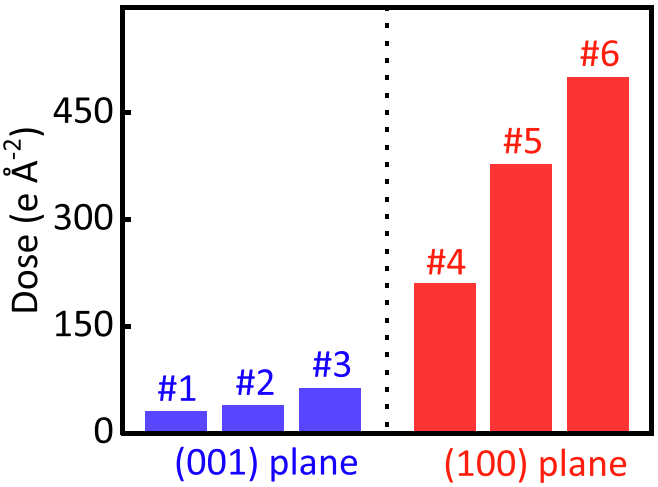

Fig. 4. (Color online) Facet-dependent electron beam sensitivity. The measured D_t values with different crystal planes exposure of $MAPbI_3$. The dose rate is 1 e $Å^{-2}$ s^{-1} at 300 kV.

We also find a facet-dependent electron beam sensitivity for $MAPbI_3$. Specifically, as shown in Fig. 4, the D_t for a (1 0 0) exposed plane ranges from 210 to 500 e $Å^{-2}$ which is about 10 times larger than a (0 0 1) exposed plane (30–41 e $Å^{-2}$) for $MAPbI_3$, obtained from Fig. S10 (online). This is because the migration barrier of iodine on (0 0 1) surface (0.32 eV) is smaller than that on (1 0 0) surface (0.45 eV), calculated by the first-principles study [37], suggesting an easier diffusion of iodine on (0 0 1) surface and relatively higher stability of (1 0 0) surface. In fact, the higher stability of (1 0 0) exposed $MAPbI_3$ surface is also consistent with Lv's study that (0 0 1) facet exhibited greater sensitivity and faster eorsion rate to water than the (1 0 0) facet [38].

We further study the effect of anion and compare the beam sensitivity of tetragonal $MAPbI_3$ and cubic $MAPbBr_3$. The D_t for $MAPbI_3$ ranges from 30 to 41 e $Å^{-2}$ (Fig. S10a–c online) which is about half of $MAPbBr_3$ (63–113 e $Å^{-2}$), acquired from Fig. S11 (online), suggesting that $MAPbBr_3$ is more stable than $MAPbI_3$ under electron beam iiradiation. The result is consistent with the conclution that $MAPbBr_3$ is more thermally and chemically stable than $MAPbI_3$ [39,40], further indicating it is reasonable to judge the stability by comparing the D_t values.

OIHPs are extremely sensitive to electron beam and it is always difficult to acqiure the atomic stucture. Our findings suggest TEM characterizations may be carried out at 300 kV and RT rather than a low voltage and a low temperature. With these guidance, we have also acquired the structure of $MAPbI_3$ at 300 kV and 25 °C, as shown in Fig. 5. At a low dose (3.1 e $Å^{-2}$), the HRTEM image (Fig. 5a) is identified to be the pristine $MAPbI_3$ judging from the corresponding fast Fourier transform (FFT) (Fig. 5b), which is consistent with the simulated ED pattern in Fig. 5c. When the summed dose increases to 24.9 e $Å^{-2}$, many additional superstructure diffraction spots appear (Fig. 5d,e), which is likely due to the ordered vacancies in $MAPbI_{2.5}$, whose simulated ED (Fig. 5f) can match the FFT, as we reported previously [7]. In fact, a few dim additional diffraction spots have already appeared even at

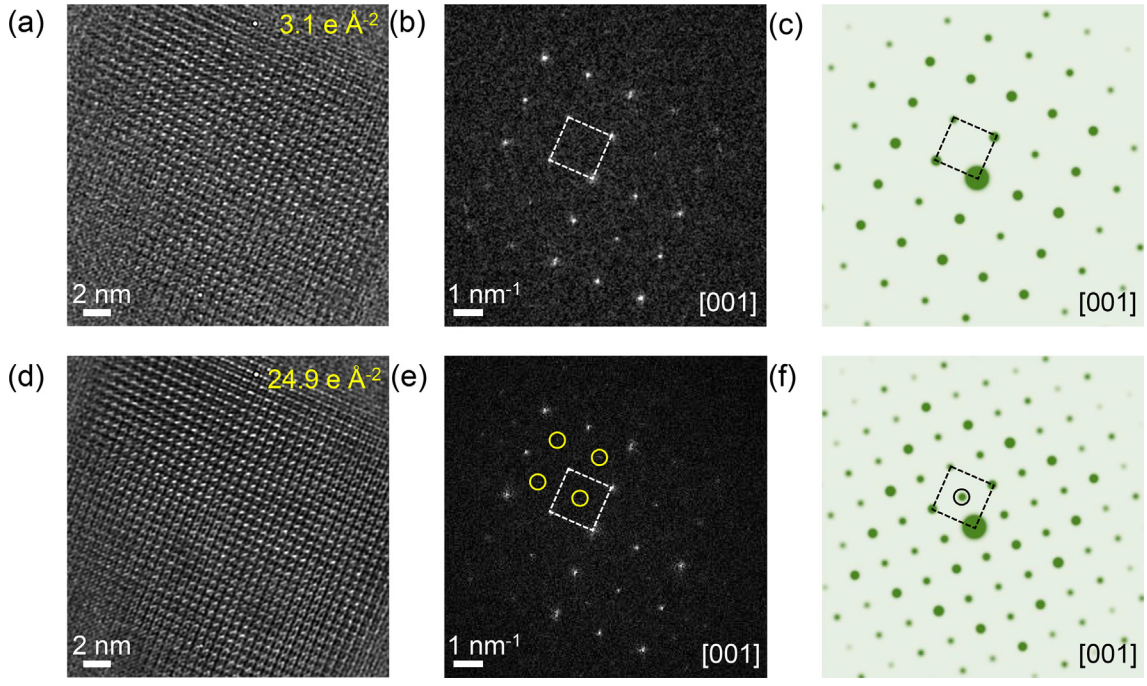

Fig. 5. (Color online) Structure of $MAPbI_3$ and superstructure. (a) HRTEM image of $MAPbI_3$, (b) the corresponding FFT pattern showing no damage occurs at this dose and (c) the simulated ED pattern. (d) HRTEM image of the superstructure, (e) the corresponding FFT pattern showing damage has already happened and (f) the simulated ED pattern. Circles highlight the additional superstructure spots.

6.2 e Å^{-2} (Fig. S12 online), suggesting several e Å^{-2} is able to induce phase transition or damage for $MAPbI_3$. Accordingly, on the one hand, extra attention should be paid to the dim additional superstructure spots that are easily ignored but indicating the phase transition when dealing with the atomic structure of $MAPbI_3$. On the other hand, extremely low dose must be used to acquire the structure of $MAPbI_3$ as well as its structure evolution.

4. Conclusion

Recently, the cryo-EM is widely believed to mitigate the electron beam damage, especially for organic materials, by lessening mass loss and the heating damage to a certain degree [41,42]. For example, the study of Li et al. [8] has inspired extensive investigations of cryo-EM for characterizing OIHPs [43,44]. While the paper was under review, a cryo-TEM work by Zhu et al. [45] reported the observation of the atomic steps of surface and stacking faults in $MAPbI_3$ at 70–100 e Å^{-2}. Our study however, suggests that for OIHPs lowering temperature by a cryo-holder cannot prevent the damage but causes a rapid crystal-amorphous transition. The inconsistency may come from the difference between diverse specimens, or the discrepancy between the cryo-holder and cryo-microscope methods. In fact, the specimens prepared for cryo-EM are naturally coated with an amorphous ice layer [46] that likely severs as a protective layer and thus slows down the beam damage, while the general cryo-holder method can only provide low-temperature without any coating layer. Nevertheless, further study is needed in future to clarify whether coating or low-temperature dominates the protection for the cryo-OIHPs. Besides the temperature effect, the recognized damage mechanism suggests a smaller damage of OIHPs is expected at a higher voltage.

Moreover, our work might shed lights on improving the performance of perovskite solar cells (PSCs). For example, we find that heating to 90 °C does not cause more severe degradation of $MAPbI_3$. Therefore, more attention can be paid to stablize the interface or other layers in PSCs to improve the high temperature performance. In addition, the facet-dependent beam sensitivity suggests that (1 0 0) surface might be more stable than (0 0 1) facet, which can also guide facet engineering to imporve the stability and performance of PSCs by growing (1 0 0)-textured perovskite films.

In summary, by using low-dose ED imaging techniques, we have investigated the optimized condition for TEM charactrizations of OIHPs. We have also quantified the threshold electron dose to acquire the pristine SAED as well as the HRTEM image of $MAPbI_3$. These findings are helpful to guide the furture TEM charactrizations. On the other hand, our work provides some valuable insights into understanding the degradation mechanism of OIHPs and can also be useful for improving the performance of PSCs.

Conflict of interest

The authors declare that they have no conflict of interest.

Acknowledgments

The work was supported by the Key Area Research and Development Program of Guangdong Province (2018B010109009), the National Key R&D Program of China (2016YFA0300804, 2016YFA0300903, and 2016YFA0201001), the National Natural Science Foundation of China (51672007, 11974023, 51575135, U1537206, and 11772207), National Equipment Program of China (ZDYZ2015-1),"2011 Program" Peking-Tsinghua-IOP Collaborative Innovation Center of Quantum Matter, Natural Science Foundation of Hebei Province for Distinguished Young Scholar (A2019210204), High Level Talent Support Project in Hebei (C201821), State Key Laboratory of Mechanics and Control of Mechanical Structures, Nanjing University of Aeronautics and Astronautics (MCMS-E-0519G04), and Youth Top-notch Talents Supporting Plan of Hebei Province. The authors acknowledge Electron Microscopy Laboratory in Peking University for the use electron microscopes.

Author contributions

Peng Gao, Jiangyu Li, Junlei Qi, and Jinjin Zhao conceived the idea and designed the experiments. Shulin Chen performed TEM related experiments with the help of Jingmin Zhang and analyzed TEM data under the direction of Peng Gao. Ying Zhang synthesized the $MAPbI_3$ single crystal films and $MAPbBr_3$ single crystals under the direction of Jinjin Zhao. Zhou Mi and Guanglei Zhang performed the SEM and XRD. Jian Cao, Jicai Feng and Junlei Qi provided crystals. Shulin Chen, Jiangyu Li and Peng Gao wrote the manuscript and all authors participated in the discussion.

Appendix A. Supplementary materials

Supplementary materials to this article can be found online at https://doi.org/10.1016/j.scib.2020.05.020.

References

[1] Kojima A, Teshima K, Shirai Y, et al. Organometal halide perovskites as visible-light sensitizers for photovoltaic cells. J Am Chem Soc 2009;131:6050–1.
[2] National Renewable Energy Laboratory (NREL). Efficiency Records Chart. https://www.nrel.gov/pv/cell-efficiency.html (Date of access: May, 2020).
[3] Wu X, Tan LZ, Shen X, et al. Light-induced picosecond rotational disordering of the inorganic sublattice in hybrid perovskites. Sci Adv 2017;3:1602388.
[4] Bryant D, Aristidou N, Pont S, et al. Light and oxygen induced degradation limits the operational stability of methylammonium lead triiodide perovskite solar cells. Energy Environ Sci 2016;9:1655–60.
[5] Kosasih FU, Ducati C. Characterising degradation of perovskite solar cells through *in-situ* and operando electron microscopy. Nano Energy 2018;47:243–56.
[6] Zhou Y, Sternlicht H, Padture NP. Transmission electron microscopy of halide perovskite materials and devices. Joule 2019;3:641–61.
[7] Chen S, Zhang X, Zhao J, et al. Atomic scale insights into structure instability and decomposition pathway of methylammonium lead iodide perovskite. Nat Commun 2018;9:4807.
[8] Li Y, Zhou W, Li Y, et al. Unravelling degradation mechanisms and atomic structure of organic-inorganic halide perovskites by cryo-EM. Joule 2019;3:2854–66.
[9] Zhu H, Fu Y, Meng F, et al. Lead halide perovskite nanowire lasers with low lasing thresholds and high quality factors. Nat Mater 2015;14:636–42.
[10] Fan Z, Xiao H, Wang Y, et al. Layer-by-layer degradation of methylammonium lead tri-iodide perovskite microplates. Joule 2017;1:548–62.
[11] Divitini G, Cacovich S, Matteocci F, et al. *In situ* observation of heat-induced degradation of perovskite solar cells. Nat Energy 2016;1:15012.
[12] Yang M, Zhou Y, Zeng Y, et al. Square-centimeter solution-processed planar $CH_3NH_3PbI_3$ perovskite solar cells with efficiency exceeding 15%. Adv Mater 2015;27:6363–70.
[13] Zhou Y, Vasiliev AL, Wu W, et al. Crystal morphologies of organolead trihalide in mesoscopic/planar perovskite solar cells. J Phys Chem Lett 2015;6:2292–7.
[14] Xiao M, Huang F, Huang W, et al. A fast deposition-crystallization procedure for highly efficient lead iodide perovskite thin-film solar cells. Angew Chem Int Ed 2014;53:9898–903.
[15] Kollek T, Gruber D, Gehring J, et al. Porous and shape-anisotropic single crystals of the semiconductor perovskite $CH_3NH_3PbI_3$ from a single-source precursor. Angew Chem Int Ed 2015;54:1341–6.
[16] Li D, Wang G, Cheng H, et al. Size-dependent phase transition in methylammonium lead iodide perovskite microplate crystals. Nat Commun 2016;7:11330.
[17] Kim TW, Shibayama N, Cojocaru L, et al. Real-time *in situ* observation of microstructural change in organometal halide perovskite induced by thermal degradation. Adv Funct Mater 2018;28:1804039.
[18] Jeangros Q, Duchamp M, Werner J, et al. *In situ* TEM analysis of organic-inorganic metal-halide perovskite solar cells under electrical bias. Nano Lett 2016;16:7013–8.
[19] Jung HJ, Kim D, Kim S, et al. Stability of halide perovskite solar cell devices: *in situ* observation of oxygen diffusion under biasing. Adv Mater 2018;30:1802769.
[20] Alberti A, Bongiorno C, Smecca E, et al. Pb clustering and PbI_2 nanofragmentation during methylammonium lead iodide perovskite degradation. Nat Commun 2019;10:2196.

[21] Rothmann MU, Li W, Zhu Y, et al. Structural and chemical changes to $CH_3NH_3PbI_3$ induced by electron and gallium ion beams. Adv Mater 2018;30:1800629.
[22] Rothmann MU, Li W, Zhu Y, et al. Direct observation of intrinsic twin domains in tetragonal $CH_3NH_3PbI_3$. Nat Commun 2017;8:14547.
[23] Zhang D, Zhu Y, Liu L, et al. Atomic-resolution transmission electron microscopy of electron beam-sensitive crystalline materials. Science 2018;359:675–9.
[24] Zhao J, Kong G, Chen S, et al. Single crystalline $CH_3NH_3PbI_3$ self-grown on FTO/TiO_2 substrate for high efficiency perovskite solar cells. Sci Bull 2017;62:1173–6.
[25] Liu Y, Yang Z, Cui D, et al. Two-inch-sized perovskite $CH_3NH_3PbX_3$ (X= Cl, Br, I) crystals: growth and characterization. Adv Mater 2015;27:5176–83.
[26] Whitfield PS, Herron N, Guise WE, et al. Structures, phase transitions and tricritical behavior of the hybrid perovskite methyl ammonium lead iodide. Sci Rep 2016;6:1–16.
[27] Quarti C, Mosconi E, Ball JM, et al. Structural and optical properties of methylammonium lead iodide across the tetragonal to cubic phase transition: implications for perovskite solar cells. Energy Environ Sci 2016;9:155–63.
[28] Diroll BT, Guo P, Schaller RD. Unique optical properties of methylammonium lead iodide nanocrystals below the bulk tetragonal-orthorhombic phase transition. Nano Lett 2018;18:846–52.
[29] Chen J, Shi T, Li X, et al. Effect of crystal structures on the stability of $CH_3NH_3PbI_3$ under humidity environment. Sol Energy 2016;136:470–4.
[30] Dang Z, Shamsi J, Akkerman QA, et al. Low-temperature electron beam-induced transformations of cesium lead halide perovskite nanocrystals. ACS Omega 2017;2:5660–5.
[31] Williams DB, Carter CB. Transmission electron microscopy: a textbook for materials science. 2nd Edition. New York: Springer; 2009.
[32] Egerton RF. Radiation damage to organic and inorganic specimens in the TEM. Micron 2019;119:72–87.
[33] Yang D, Ming W, Shi H, et al. Fast diffusion of native defects and impurities in perovskite solar cell material $CH_3NH_3PbI_3$. Chem Mater 2016;28:4349–57.
[34] Egerton RF, Li P, Malac M. Radiation damage in the TEM and SEM. Micron 2004;35:399–409.
[35] Ugurlu O, Haus J, Gunawan AA, et al. Radiolysis to knock-on damage transition in zeolites under electron beam irradiation. Phys Rev B 2011;83:113408.
[36] Egerton RF. Control of radiation damage in the TEM. Ultramicroscopy 2013;127:100–8.
[37] Haruyama J, Sodeyama K, Han L, et al. First-principles study of ion diffusion in perovskite solar cell sensitizers. J Am Chem Soc 2015;137:10048–51.
[38] Lv Q, He W, Lian Z, et al. Anisotropic moisture erosion of $CH_3NH_3PbI_3$ single crystals. CrystEngComm 2017;19:901–4.
[39] Zuo Z, Ding J, Zhao Y, et al. Enhanced optoelectronic performance on the (110) lattice plane of an $MAPbBr_3$ single crystal. J Phys Chem Lett 2017;8:684–9.
[40] Shahbazi M, Wang H. Progress in research on the stability of organometal perovskite solar cells. Sol Energy 2016;123:74–87.
[41] Li Y, Li Y, Pei A, et al. Atomic structure of sensitive battery materials and interfaces revealed by cryo-electron microscopy. Science 2017;358:506–10.
[42] Wiktor C, Turner S, Zacher D, et al. Imaging of intact MOF-5 nanocrystals by advanced TEM at liquid nitrogen temperature. Micropor Mesopor Mat 2012;162:131–5.
[43] Shi L, Wang J, Zhou L, et al. Facile *in-situ* preparation of $MAPbBr_3$@UiO-66 composites for information encryption and decryption. J Solid State Chem 2020;282:121062.
[44] Herzing AA, DeLongchamp DM. Cold Microscopy solves hot problems in energy research. Matter 2019;1:1106–7.
[45] Zhu Y, Gui Z, Wang Q, et al. Direct atomic scale characterization of the surface structure and planar defects in the organic-inorganic hybrid $CH_3NH_3PbI_3$ by Cryo-TEM. Nano Energy 2020;73:104820.
[46] Toyoshima C, Sasabe H, Stokes DL. Three-dimensional cryo-electron microscopy of the calcium ion pump in the sarcoplasmic reticulum membrane. Nature 1993;362:469–71.

Shulin Chen is currently a Ph.D. candidate in School of Materials Science and Engineering, Harbin Institute of Technology. He received his Bachelor's degree from Harbin Institute of Technology in 2015. He joined Prof. Peng Gao's group in February 2016 as a joint Ph.D. candidate. His research interest is probing structure-property relationships of energy storage and conversion devices via using TEM.

Jinjin Zhao is a professor in Shijiazhuang Tiedao University. She obtained her Ph.D. degree in Materials Physics and Chemistry from Shanghai Institute of Ceramics, Chinese Academy of Sciences in 2010. She did her visiting doctoral studies from Max Plank Institute of Colloids and Interfaces from 2007 to 2008, and visiting scholar at the University of Washington from 2015 to 2016, and visited City University of Hong Kong in 2019. She held faculty appointment in Shijiazhuang Tiedao University. She is interested in probing instability mechanism in perovskite devices.

Junlei Qi is a full professor in School of Materials Science and Engineering, Harbin Institute of Technology, Harbin, China. He received his B.S. and Ph.D. degrees from Jilin University in 2005 and 2010. He was a visiting scholar at the University of Tokyo (2012–2013) to investigate single-crystal graphene micro-nano device manufacturing. His current interests focus on carbon nanomaterials, metal matrix composites and transition metal compounds for energy storage devices.

Jiangyu Li obtained his B.E. degree in 1994 from the Department of Materials Science and Engineering, Tsinghua University, and Ph.D. degree in 1998 from the Department of Mechanical Engineering, University of Colorado-Boulder. He works in the general field of mechanics of materials, focusing on advanced scanning probe microscopy and its applications in functional materials.

Peng Gao is an assistant professor in School of Physics, Peking University, China. He received his Ph.D. degree in Condensed Mater Physics from the Institute of Physics, Chinese Academy of Sciences in 2010. He was a post-doctor in University of Michigan (2010–2013), research associate in Brookhaven National Lab (2013–2014), research fellow and Japan Society for the Promotion of Science (JSPS) foreign fellow in University of Tokyo (2014–2015). He joined in Peking University in 2015. His main research interests is atomic structure, excitation state, nonequilibrium state of interfaces in ferroics, solid-state ionics and low-dimensional quantum materials.